

Efficient experimental design of high-fidelity three-qubit quantum gates via genetic programming

Amit Devra,¹ Prithviraj Prabhu,² Harpreet Singh,¹ Arvind,¹ and Kavita Dorai¹

¹*Department of Physical Sciences, Indian Institute of Science Education & Research (IISER) Mohali, Sector 81 SAS Nagar, Punjab 140306 India.*

²*Sri Sivasubramaniya Nadar College of Engineering, Kalavakkam, Chennai, Tamil Nadu 603110 India.*

We have designed efficient quantum circuits for the three-qubit Toffoli (controlled-controlled NOT) and the Fredkin (controlled-SWAP) gate, optimized via genetic programming methods. The gates thus obtained were experimentally implemented on a three-qubit NMR quantum information processor, with a high fidelity. Toffoli and Fredkin gates in conjunction with the single-qubit Hadamard gates form a universal gate set for quantum computing, and are an essential component of several quantum algorithms. Genetic algorithms are stochastic search algorithms based on the logic of natural selection and biological genetics and have been widely used for quantum information processing applications. The numerically optimized rf pulse profiles of the three-qubit quantum gates achieve $> 99\%$ fidelity. The optimization was performed under the constraint that the experimentally implemented pulses are of short duration and can be implemented with high fidelity. Therefore the gate implementations do not suffer from the drawbacks of rf offset errors or debilitating effects of decoherence during gate action. We demonstrate the advantage of our pulse sequences by comparing our results with existing experimental schemes.

PACS numbers: 03.67.-a, 03.67.Ac, 03.67.Lx

I. INTRODUCTION

Quantum technologies that have been proposed to build quantum computers should be able to achieve a high degree of control over a universal set of quantum gates that form the basic elements of quantum circuits [1]. Any quantum computing circuit can be realized using a universal set of two-qubit gates and a set of local unitaries [2]. However using this basic set of single- and two-qubit gates to decompose multiqubit unitary propagators for large qubit registers, leads to problems of scalability and decoherence due to long operation times of the circuits [3]. Hence, the idea of multi-level quantum logic was developed which used three- and four-qubit quantum gates to considerably simplify the quantum circuit [4, 5].

Three-qubit gates such as the Toffoli gate (which is equivalent to controlled-controlled-NOT operation) and the Fredkin gate (which is equivalent to a controlled-SWAP operation) play an important role in quantum circuits [6], fingerprinting [7], optimal cloning [8] and quantum error correction [9, 10]. The Fredkin gate was discussed early on as a useful gate for optical implementations of quantum computing [11, 12]. The Toffoli and the Fredkin gates, in conjunction with the single-qubit Hadamard gate, form a universal set of quantum gates [13, 14]. Previous implementations of these universal three-qubit gates relied on their decomposition into sets of single- and two-qubit gates [15, 16]. Efficient construction of three- and four-qubit gates using an optimal set of global entangling gates has been recently explored [17], and a machine learning type of algorithm has been used to design high-fidelity single-shot three-qubit gates which do not require prior decomposition into sets of two-qubit gates [18, 19].

Three- and four-qubit gates were experimentally realized early on in NMR quantum computing by several groups [20–23]. The Toffoli gate has been experimentally implemented using trapped ions [24] and circuit QED [25] and superconducting qubits [26, 27]. Several studies of the Toffoli gate have focused on its experimental realization using optical setups [28–30]. Other implementations of the Toffoli gate include an optimal version using a reduced set of two-qubit gates [31, 32]. The Fredkin (controlled-SWAP) gate was recently experimentally realized using photonic qubits [33].

Several optimization techniques have been successfully developed for quantum control such as strongly modulated pulses [34], GRAPE optimization [35, 36], sequential convex programming [37] and optimal dynamical discrimination [38]. A novel set of optimization techniques broadly categorized as ‘Genetic Algorithms (GAs)’, have also been proposed as a means to achieve a global minimum for the optimization [39]. GAs borrow their optimization protocol from the basic tenets of evolutionary biology, wherein the breeding strategy of a population is to increase the fitness levels and offspring-producing capability of individuals by crossing over of genetic information [40]. In quantum information processing, GAs have been used to optimize quantum algorithms [41–43] and quantum entanglement [44], for optimal dynamical decoupling [45], and to optimize unitary transformations for a general quantum computation [46, 47].

In this work, we explore the efficacy of GAs in optimizing the Toffoli and Fredkin gates alongwith a set of single-qubit gates, on a three-qubit NMR quantum information processor. We design an implementation of these gates which uses only “hard” (*i.e.* short duration) rf pulses of arbitrary flip angles and phases, punctuated by inter-

vals of evolution under the system Hamiltonian. We are hence able to substantially avoid the pitfalls associated with “soft” shaped NMR pulses, namely pulse calibration errors and degradation due to decoherence occurring during the long gate times of such pulses. The constraints are put in from practical considerations, whereby we want to design the gate using only a certain kind of short duration rf pulses, and then genetic algorithms are used to optimize the protocol. We compared our experimental results with previous NMR implementations of these three-qubit gates using standard transition-selective shaped pulses. We demonstrate that our scheme is substantially better, with obtained experimental fidelities $\approx 14\%$ higher as compared to the standard implementations and also report a 5-6 times savings in gate implementation time as compared to the standard implementations. Our scheme is general and can be implemented on any quantum hardware to generate circuits for three-qubit gates of high fidelity.

The material in this paper is arranged as follows: In Section II we describe the optimization scheme based on GAs. In Section III we discuss the implementation of optimized gates on an NMR system of three qubits with Section III A containing the details of the NMR system, Section III B describing the optimized implementation of a 90° pulse, Section III C the implementation of a two-qubit CNOT gate. While Sections III D and III E describe the implementation of the optimized Fredkin and Toffoli gates respectively, in Section III F we compare our results with standard implementations of these gates. Section IV offers some concluding remarks.

II. NUMERICAL OPTIMIZATION OF THREE-QUBIT GATES VIA GENETIC PROGRAMMING

Unitary operators corresponding to controlled operations and to quantum gates can be implemented on an NMR quantum information processor by a suitable set of radiofrequency pulses of a specific frequency, amplitude and phase, interspersed with delays which correspond to free evolution under the system Hamiltonian. The problem of numerical optimization of any quantum gate can hence be recast as an optimization problem in genetic programming, wherein the fitness function to be optimized depends on the target unitary operator, with its corresponding set of pulse parameters and delay times. The fitness function which determines the relative distance between two operators, is defined in our scenario as [47, 48]:

$$\mathcal{F} = \frac{|\text{Tr}(U_{\text{tgt}}U_{\text{opt}}^\dagger)|}{\sqrt{\text{Tr}(U_{\text{tgt}}U_{\text{tgt}}^\dagger)\text{Tr}(U_{\text{opt}}U_{\text{opt}}^\dagger)}} \quad (1)$$

where U_{tgt} is the target unitary operator of the desired gate to be optimized and U_{opt} is the actual operator generated by the GA optimization. The fitness function is

normalized such that when $U_{\text{opt}}=U_{\text{tgt}}$, the fitness has the maximum value of unity.

The derived unitary operator of the gate to be optimized, U_{opt} , is defined as:

$$U_{\text{opt}} = \prod_{l=1}^N \exp[-i(\mathcal{H}_{\text{NMR}} + \Omega I_{\phi_l k})\tau_l] \exp[-i\mathcal{H}_{\text{NMR}}\delta_l] \quad (2)$$

$$I_{\phi_l} = \frac{1}{2}(\sigma_x \cos \phi_l + \sigma_y \sin \phi_l)$$

where Ω denotes the amplitude of the rf pulse, ϕ_l is the phase of the l th rf pulse, τ_l is the pulse length, δ_l denotes an evolution period under the system Hamiltonian, and σ_x and σ_y are the Pauli x and y matrices respectively. The first term in the expression for the desired unitary operator U_{opt} (Eqn. 2) describes the system and RF Hamiltonians, while the second term describes the evolution under the the system Hamiltonian. The system Hamiltonian \mathcal{H}_{NMR} in the rotating frame is given by

$$\mathcal{H}_{\text{NMR}} = -\pi \sum_{i=1}^n (\nu_i - \nu_{r,f}^i) \sigma_z^i + \sum_{i<j,=1}^n \frac{\pi}{2} J_{ij} \sigma_z^i \sigma_z^j \quad (3)$$

where n denotes the number of spins, ν_i and $\nu_{r,f}^i$ are the chemical shift and the rotating frame frequencies respectively, J_{ij} are the scalar coupling constants and σ_z is the Pauli z matrix.

We choose to decompose the desired unitary operator U_{opt} as a set of N hard (*i.e.* high-power, very short duration) rf pulses, each of fixed amplitude Ω , pulse length τ_l and phase ϕ_l , and a set of N delays, each of interval δ_l in duration. This set of pulses and delays denotes the basic propagator (Fig. 1). These optimal pulse phase,

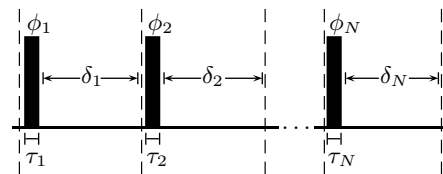


FIG. 1. Desired unitary propagator is represented by a set of N pulses of pulse width τ_l and phase ϕ_l , punctuated by N delays of interval δ_l ($l = 1 \dots N$).

pulse width and delay values (which together constitute one possible solution to the optimization problem) can be encoded in the form of a matrix of order $N \times 4$ where the number of rows (N) specifies the number of operations that the desired unitary operator is decomposed into. By increasing the number of rows, we increase the accuracy and control. The values of the four columns of the matrix are detailed below:

- **Column 1:** represents the width (τ) of a hard pulse, which is used to tune the value of the angle of rotation of the pulse ($\theta \in \{0, 2\pi\}$).

- **Column 2 and 3:** The phase of rotation of the rf pulse is represented in these two columns. The second column takes the values either 0 or 1, implying a positive or negative phase ($\phi \in \{0, \pi\}$ or $\phi \in \{-\pi, 0\}$, respectively). The third column contains the entire range of ϕ values from $\{0, 2\pi\}$.
- **Column 4:** The values in this column represent the time evolution δ_l between hard pulses. The maximum value that an element in this column can assume is relative to the type of gate chosen. A Fredkin gate inherently requires more time than a CNOT gate, and hence will be given more freedom in choosing delay lengths.

Due to accuracy constraints imposed by the NMR hardware on which the gates are implemented, we can only obtain a resolution of 0.01 degrees for the phase, and a resolution of $1\mu\text{s}$ for the delay. Hence the values in our results are discretized accordingly. It should also be noted that the power of each hard rf pulse is fixed and is not optimized.

As the first step in the genetic algorithm, an initial population of solutions, *i.e.* n ‘randomly chosen chromosomes’ is created. Considering we run the algorithm using a variable number of rows, we must first decide upon a suitable population size to run the algorithm with. As the number of rows increases, so does the time taken to convert a matrix of rf pulses to a gate matrix. We thus used population sizes ranging from 350 to 750, for rows ranging from 3-20. There are three main operations which form the backbone of the genetic algorithm as described below [39]:

- **Selection:** Selecting individuals for crossover and mutation processes is important as it dictates the direction taken by the population in the fitness landscape [39]. We initially use a low selection pressure in order to explore all possible candidate solutions. If a viable solution is recognized, the intensity of the selection pressure is increased, to allow for exploitation of neighbors of the recognized solution. After attempting existing selection mechanisms such as roulette, rank, tournament and stochastic acceptance [49], we devised our own selection mechanism which we call “Luck-Choose”. The operation involves first multiplying pseudo-randomly generated weights to the fitness values of all individuals, and subsequently determining the highest among the output values. Using the Luck-Choose method, the algorithm converged to a solution much faster.
- **Crossover:** The crossover operation in the genetic algorithm method swaps congruent parts of individual members of the population as follows: Two members are chosen from the population using the Luck-Choose selection method. Two numbers are randomly chosen within the maximum number of rows, and two numbers are randomly chosen within the maximum number of columns. The first number of each corresponds to the starting point of the crossover and the second number corresponds to the end point. Using the above four

numbers we create a rectangular sub-matrix, which is swapped between both the selected individuals. In addition, we added another operation called *flip* in order to address the problem of non-commutativity of rf pulses. The *flip* operation selects a single member using the Luck-Choose method and swaps its constituent rows.

- **Mutation:** This operation depends heavily on the amount of stochastic noise required. Stochastic noise adds a random amount of noise to ensure that the algorithm does not stagnate at any of the local optima. In the initial stages, low stochastic noise is preferred, so the mutation operation may be disabled. However after the algorithm explores the population landscape through a few generations, the chances of getting stuck in local optima increase. The probability of mutations is then increased in steps upto a threshold value, above which the stochastic noise would only serve to drive candidate solutions away from the global optimum. Mutation takes a single member, selected using the Luck-Choose method, and changes all its data values.

After running the genetic algorithm, outputs are obtained with fidelities in the lower 0.80 range. In order to increase the fidelity, we used the concept of a localized optimizer, which is a GA tool that optimizes only within a very small region of the fitness landscape. This is done by localizing the range of values that constituent chromosomes can take. As the maximum fidelity increases, we increase the selection pressure to further minimize the region of optimization of the algorithm, in the fitness landscape. The chromosomes from the main optimizer, which yield fidelity greater than 0.8 are then passed through this local optimizer to increase the fidelity. In the general case, we let the local optimizer run for 1000 seconds. If the fidelity crossed 0.99, the solution was deemed acceptable. In certain cases, local optimizer runtimes were further increased, to increase the final fidelity. Table I gives details of the runtime per iteration in the main and local optimizers, as well as the corresponding count of Floating Point Operations per Second (FLOPS), for the optimization of a 90° spin-selective rf pulse. All the rows for which the pulse duration is mentioned in the table have a fidelity greater than 0.99. The genetic algorithm was performed using MATLAB [50]. An iteration of the program running the algorithm for 15 rows and 500 chromosomes, took an average time of 3 hours using a single core for processing, on an i7-4700MQ processor with 8 GB of RAM. For parallel processing, the Parallel Computing Toolbox was used, enabling us to run 6 iterations simultaneously on 6 virtual cores for approximately 4 hours. This reduced the average runtime per iteration to approximately 40 minutes. The local optimizer however was run from 10 minutes to 15 hours depending on the final fidelity required and the fidelity of the starting matrix.

Row No.	Main Optimizer Time(s)/GFLOPS	Local Optimizer Time(s)/GFLOPS	Pulse Duration
1	277.8/901.5	NA	NA
2	559.1/1814.2	NA	NA
3	871.3/2827.3	978/3173.6	101.4 μ s
4	1183.8/3841.4	46.16/149.8	146.8 μ s
5	1435.8/4656.5	59.66/193.6	164.8 μ s
6	1751.5/5683.6	28.5/92.5	253.7 μ s
7	2005.6/6508.1	23.2/75.3	243.7 μ s
8	2176.6/7063.1	19.2/62.3	292.3 μ s

TABLE I. Table of total optimization time and total pulse duration against the number of rows for the optimization of a 90° spin-selective rf pulse. The optimization time per iteration is shown, alongwith the corresponding number of FLOPs used.

III. EXPERIMENTAL IMPLEMENTATION OF NUMERICALLY OPTIMIZED GATES

A. Experimental NMR qubits

The three fluorine (^{19}F) spins of the molecule iodotrifluoroethylene were used to encode the three qubits (Fig. 2). The three qubits were initialized into a pseu-

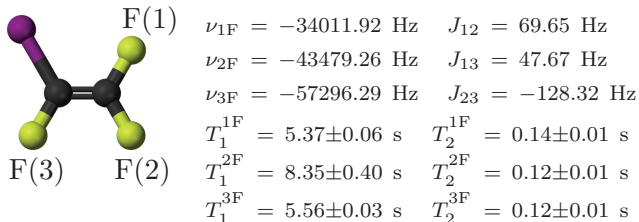


FIG. 2. Structure of iodotrifluoroethylene molecule with measured values of chemical shifts (ν_i) and scalar couplings (J).

dopure state $|110\rangle$ via the spatial averaging technique [51] with the density operator given by

$$\rho_{110} = \frac{1-\epsilon}{8}I + \epsilon|110\rangle\langle 110| \quad (4)$$

where thermal polarization (ϵ) is approximately 10^{-5} and I is a 8×8 identity matrix. The experimentally created pseudopure state was tomographed with a fidelity of 0.97. All the experimental density matrices were reconstructed using a reduced tomographic protocol [52] and maximum likelihood estimation [53] with the set of operations given by $\{III, IYY, IYY, YII, XYX, XXY, XX X\}$, where I is the identity operation, X and Y are the single spin angular momentum operators which can be implemented by applying a $\pi/2$ pulse on the corresponding spin. The operators for tomographic protocols were numerically optimized using genetic programming, each having a length of approximately 200 μ s and an average fidelity of ≥ 0.99 .

The fidelity of the experimental density matrix was computed by measuring the projection between the theoretically expected and experimentally measured states using the Uhlmann-Jozsa fidelity measure [54, 55]

$$F = \text{Tr} \left(\sqrt{\sqrt{\rho_{\text{th}}}\rho_{\text{exp}}\sqrt{\rho_{\text{th}}}} \right) \quad (5)$$

where ρ_{th} and ρ_{exp} denote the theoretical and experimental density matrices respectively.

Since we used a system of three homonuclear (same spin species) spins, the control on all three spins happens simultaneously and the optimization operator U_{opt} is modified as:

$$U_{\text{opt}} = \prod_{l=1}^N \exp[-i(\mathcal{H}_{\text{NMR}} + \Omega(I_{\phi_1} + I_{\phi_2} + I_{\phi_3}))\tau_l] \exp[-i\mathcal{H}_{\text{NMR}}\delta_l] \quad (6)$$

The amplitude (Ω) of the hard rf pulse was kept fixed at 120.88×10^3 rad/s, the hard pulse flip angle was taken in range of $\{0, 3\pi/2\}$ and range for length of the pulse (τ) was adjusted according to these two factors. The value of the delay between the pulses was chosen depending upon the unitary being optimized.

B. Implementation of 90° selective rf pulse

l	$\tau_l(\mu\text{s})$	ϕ_l	$\delta_l(\mu\text{s})$
1	16	87.65	21
2	33	269.97	21
3	16	92.29	0

TABLE II. Table representing the pulse sequence for selective pulse. First column represents the number of propagators. The second, third and fourth columns give the pulse width (τ), phase (ϕ) and delay (δ) values, respectively.

To rotate a single spin in a homonuclear system we need a selective excitation pulse. We optimized the pulse sequence via genetic algorithm for a 90° selective pulse on the third qubit along the Y-axis, using only hard pulses and delays. The unitary for the selective pulse is given by,

$$U_{\text{tgt}} = \frac{1}{\sqrt{2}} \begin{bmatrix} 1 & -1 & 0 & 0 & 0 & 0 & 0 & 0 \\ 1 & 1 & 0 & 0 & 0 & 0 & 0 & 0 \\ 0 & 0 & 1 & -1 & 0 & 0 & 0 & 0 \\ 0 & 0 & 1 & 1 & 0 & 0 & 0 & 0 \\ 0 & 0 & 0 & 0 & 1 & -1 & 0 & 0 \\ 0 & 0 & 0 & 0 & 1 & 1 & 0 & 0 \\ 0 & 0 & 0 & 0 & 0 & 0 & 1 & -1 \\ 0 & 0 & 0 & 0 & 0 & 0 & 1 & 1 \end{bmatrix} \quad (7)$$

The optimized pulse sequence for this unitary is given in Table II. The pulse sequence was obtained with a theoretical fidelity of 0.995 with a pulse duration of 107 μ

s. The numerically optimized pulse sequence was experimentally implemented on an initial thermal equilibrium state, and the result is shown in Fig. 3. There is a sub-

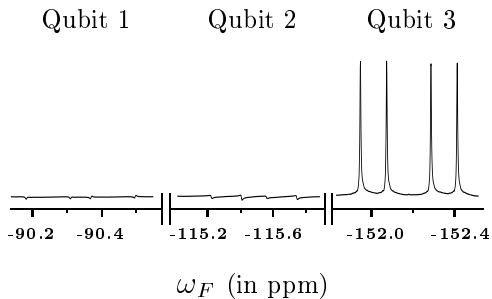


FIG. 3. Experimental implementation of a numerically optimized 90° selective pulse on the third qubit along the Y -axis, applied on a thermal equilibrium state.

stantial advantage in the much shorter duration of the optimized selective pulse which is in μs as compared to the standard pulses which usually take tens of milliseconds, depending on the system interactions. The spectra in Figure 3 show a clean excitation of the third qubit, with no spillover excitation of the other two qubits.

C. Implementation of CNOT gate

Since the interactions in NMR are always “on”, it is most often non-trivial to implement a two-qubit gate in an N qubit system, while doing nothing on the other ($N-2$) qubits in the system, as compared to implementing the same two-qubit gate in a system of two NMR qubits [56]. We hence optimized the two-qubit CNOT gate on our three-qubit system, with the first qubit considered the control qubit while the second qubit was considered the target qubit. The corresponding unitary matrix is given by

$$U_{\text{tgt}} = \begin{bmatrix} 1 & 0 & 0 & 0 & 0 & 0 & 0 & 0 \\ 0 & 1 & 0 & 0 & 0 & 0 & 0 & 0 \\ 0 & 0 & 1 & 0 & 0 & 0 & 0 & 0 \\ 0 & 0 & 0 & 1 & 0 & 0 & 0 & 0 \\ 0 & 0 & 0 & 0 & 0 & 0 & 1 & 0 \\ 0 & 0 & 0 & 0 & 0 & 0 & 0 & 1 \\ 0 & 0 & 0 & 0 & 1 & 0 & 0 & 0 \\ 0 & 0 & 0 & 0 & 0 & 1 & 0 & 0 \end{bmatrix} \quad (8)$$

The optimized pulse sequence for this quantum gate is shown in Table III, and was obtained with a theoretical fidelity of 0.993 with a pulse duration of 7 ms.

The pulse sequence was experimentally implemented on an initially prepared pseudopure state $|110\rangle$. The final state was $|100\rangle$ as expected, with an experimental fidelity of 0.97. The experimentally tomographed results are shown in Figure 4.

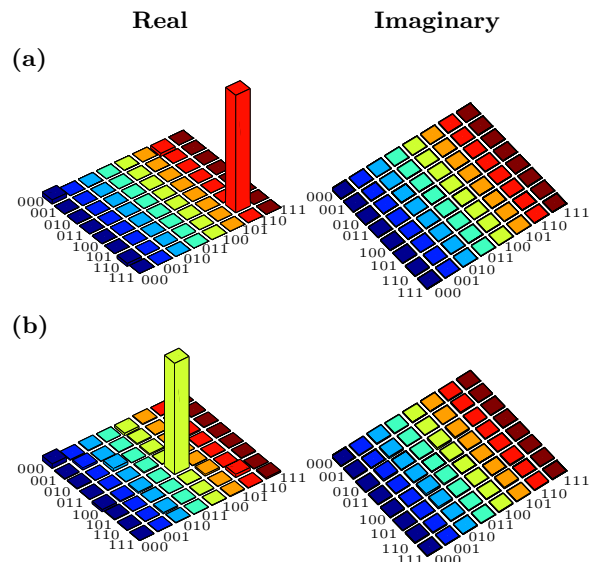


FIG. 4. Real (left) and imaginary (right) parts of the experimental tomographs of (a) Initial $|110\rangle$ state. (b) After a CNOT gate applied on the $|110\rangle$ state.

l	$\tau_1(\mu\text{s})$	ϕ_1	$\delta_1(\mu\text{s})$	l	$\tau_1(\mu\text{s})$	ϕ_1	$\delta_1(\mu\text{s})$
1	30	321.81	277	11	4	271.97	305
2	33	320.75	69	12	39	329.86	11
3	3	59.02	1	13	14	352.56	83
4	39	66.28	636	14	24	359.89	657
5	29	306.06	292	15	1	2.52	1748
6	9	302.12	19	16	6	55.02	69
7	39	312.81	1755	17	4	312.45	2
8	11	294.12	1	18	37	309.7	96
9	39	296.16	636				
10	1	157.81	256				

TABLE III. Table representing the pulse sequence for a two-qubit CNOT gate. The first column represents the number of propagators. The second, third and fourth columns represent the pulse width (τ), phase (ϕ) and delay (δ) values, respectively.

D. Implementation of Fredkin gate

We optimized the three-qubit Fredkin gate (corresponding to a controlled-SWAP operation) in a single shot *i.e.* without breaking it down into other unitaries, and using only a set of hard pulses and delays. The first qubit was designated as a control qubit and if the control qubit is 1, then the other two qubits swap their states. The unitary matrix corresponding to the Fredkin gate is

given by

$$U_{\text{tgt}} = \begin{bmatrix} 1 & 0 & 0 & 0 & 0 & 0 & 0 & 0 \\ 0 & 1 & 0 & 0 & 0 & 0 & 0 & 0 \\ 0 & 0 & 1 & 0 & 0 & 0 & 0 & 0 \\ 0 & 0 & 0 & 1 & 0 & 0 & 0 & 0 \\ 0 & 0 & 0 & 0 & 1 & 0 & 0 & 0 \\ 0 & 0 & 0 & 0 & 0 & 0 & 1 & 0 \\ 0 & 0 & 0 & 0 & 0 & 1 & 0 & 0 \\ 0 & 0 & 0 & 0 & 0 & 0 & 0 & 1 \end{bmatrix} \quad (9)$$

The optimized pulse sequence for this gate is shown in Table IV, and was obtained with a fidelity 0.99 and a pulse duration of 51 ms. The pulse sequence was ex-

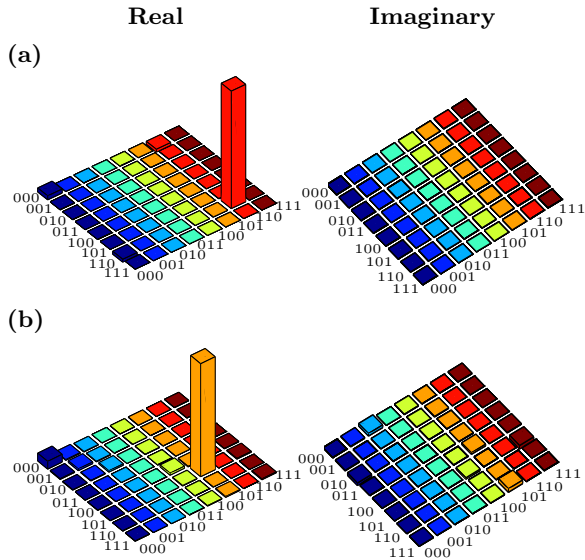


FIG. 5. Real (left) and imaginary (right) parts of the experimental tomographs of (a) Initial $|110\rangle$ state. (b) After Fredkin gate applied on the $|110\rangle$ state.

l	$\tau_1(\mu\text{s})$	ϕ_1	$\delta_1(\text{ms})$	l	$\tau_1(\mu\text{s})$	ϕ_1	$\delta_1(\text{ms})$
1	29	108.63	1.584	11	10	186	1.569
2	20	200.75	3.712	12	30	170.75	1.592
3	11	258.7	0.639	13	17	4.55	3.269
4	25	197.31	1.075	14	21	188.17	2.184
5	9	172.69	4.568	15	28	36.37	2.152
6	19	188.99	1.964	16	21	330.83	4.423
7	31	265.02	4.416	17	7	46.59	2.194
8	27	100.22	2.161	18	14	102.17	3.066
9	12	86.57	3.276	19	28	295.24	1.574
10	32	233.09	2.194	20	13	126.96	3.720

TABLE IV. Table representing the pulse sequence for the Fredkin gate. The first column represents the number of propagators. The second, third and fourth columns represent the pulse width (τ), phase (ϕ) and delay (δ), respectively.

perimentally implemented on an initial state $|110\rangle$. The

output state was $|101\rangle$ with an experimental fidelity of 0.96. The experimentally tomographed results are shown in Figure 5.

E. Implementation of Toffoli gate

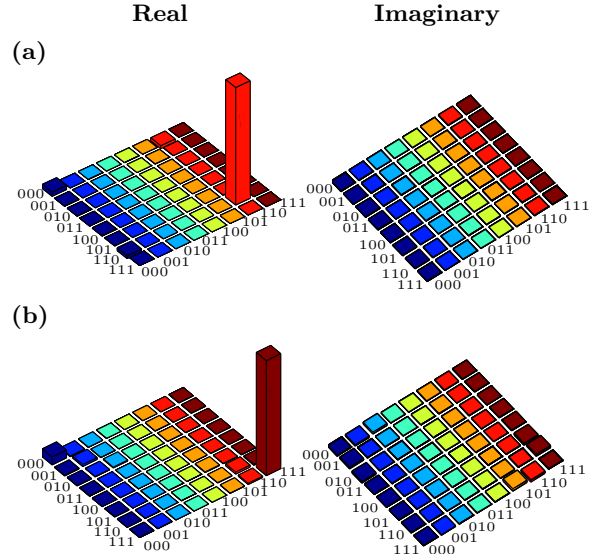


FIG. 6. Real (left) and imaginary (right) parts of the experimental tomographs of (a) Initial $|110\rangle$ state. (b) After a Toffoli gate applied on the $|110\rangle$ state.

The first two qubits of this gate were considered as the control qubits while the third qubit was designated the target qubit. The unitary matrix corresponding to this gate is given by

$$U_{\text{tgt}} = \begin{bmatrix} 1 & 0 & 0 & 0 & 0 & 0 & 0 & 0 \\ 0 & 1 & 0 & 0 & 0 & 0 & 0 & 0 \\ 0 & 0 & 1 & 0 & 0 & 0 & 0 & 0 \\ 0 & 0 & 0 & 1 & 0 & 0 & 0 & 0 \\ 0 & 0 & 0 & 0 & 1 & 0 & 0 & 0 \\ 0 & 0 & 0 & 0 & 0 & 1 & 0 & 0 \\ 0 & 0 & 0 & 0 & 0 & 0 & 0 & 1 \\ 0 & 0 & 0 & 0 & 0 & 0 & 0 & 1 \end{bmatrix} \quad (10)$$

The numerically optimized sequence for this gate is shown in Table V and was obtained with a fidelity of 0.995 and a pulse duration of 27 ms. The pulse sequence was experimentally implemented on an initially prepared pseudo-pure state $|110\rangle$. The final state was $|111\rangle$ as expected, and had an experimental fidelity of 0.93. The experimentally tomographed results are shown in Figure 6.

To check the robustness of the numerically optimized pulse sequences we considered two types of errors: offset errors and flip angle or pulse miscalibration errors. Figure 7 shows the variation of fidelity with the offset frequency (Hz) and flip angle (deg) for the different gates.

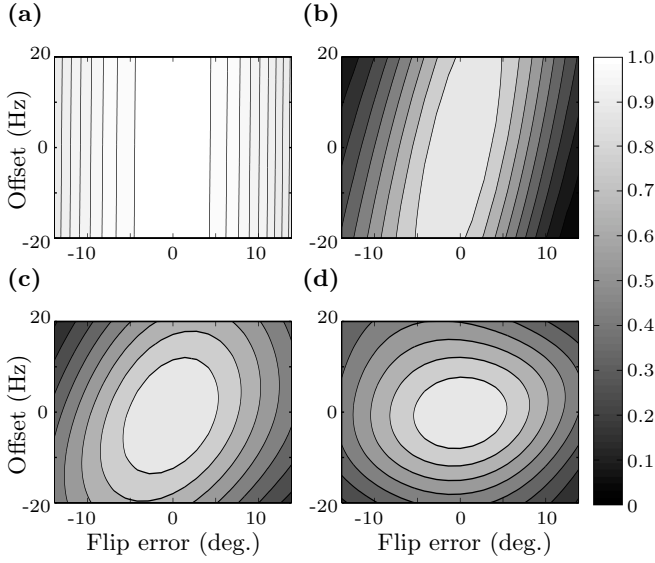


FIG. 7. Robustness of pulse sequences corresponding to (a) 90° selective pulse (b) CNOT gate (c) Fredkin gate and (d) Toffoli gate. The x and y axes represent the error in flip angle (deg) and the offset (Hz), respectively.

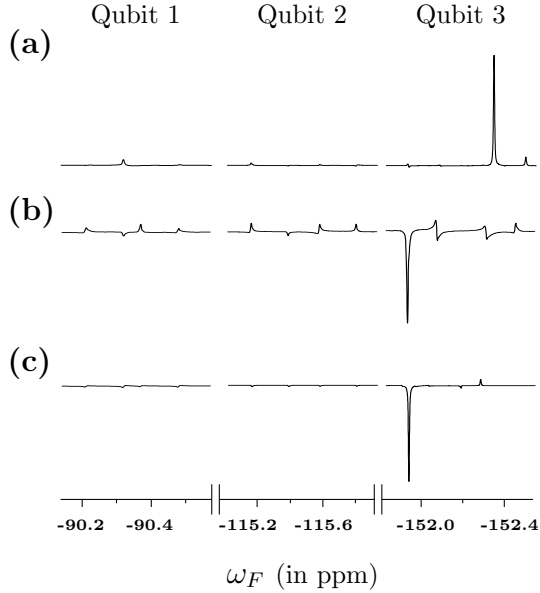


FIG. 8. NMR spectra of (a) Pseudopure state $|110\rangle$; (b) after the implementation of a Fredkin gate on the $|110\rangle$ state using transition-selective pulses; (c) after the implementation of a Fredkin gate on the $|110\rangle$ state using pulses optimized by the genetic algorithm method.

We checked the fidelity variation for the range ± 20 for offset and ± 14 for flip errors. The 90° selective rf pulse is most robust of all the other gates (as is to be expected since it is a single-qubit gate), the fidelity for this is above 0.90 for the area inside the points $(\pm 12.5, \pm 19.6)$. The two-qubit CNOT gate has fidelity > 0.9 for the area inside the points $(-5.2, -20)$, $(1.2, -20)$, $(4.7, 20)$ and $(-1.2, 20)$.

l	$\tau_1(\mu\text{s})$	ϕ_1	$\delta_1(\mu\text{s})$	l	$\tau_1(\mu\text{s})$	ϕ_1	$\delta_1(\mu\text{s})$
1.	32	243.22	539	11.	15	215.55	2487
2.	27	138.58	546	12.	27	308.2	550
3.	39	2.47	499	13.	32	326.82	513
4.	36	320.89	3488	14.	13	122.09	541
5.	32	352.29	2495	15.	4	332.61	2518
6.	34	355.84	536	16.	24	354.12	546
7.	37	175.98	1938	17.	36	310.6	3806
8.	29	20.45	1957	18.	32	210.97	1971
9.	34	354.75	542	19.	30	3.74	504
10.	18	297.71	564	20.	38	338.48	565

TABLE V. Table representing the pulse sequence for the Toffoli gate. The first column represents the number of propagators. The second, third and fourth columns represent the pulse width (τ), phase (ϕ) and delay (δ), respectively.

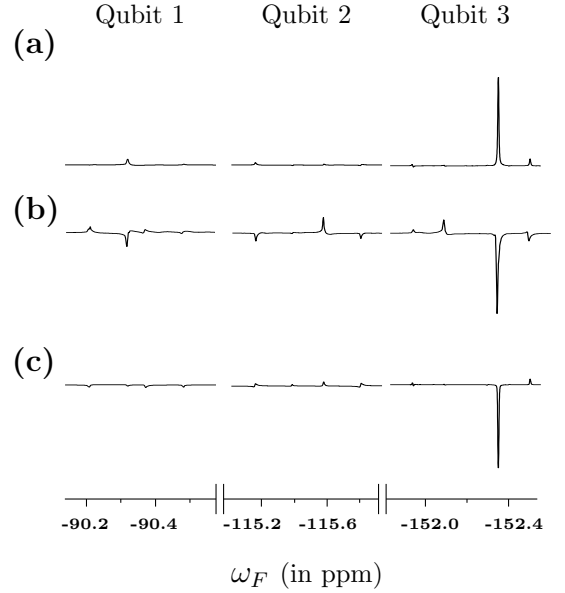


FIG. 9. NMR spectra of (a) Pseudopure state $|110\rangle$; (b) after the implementation of a Toffoli gate on the $|110\rangle$ state using transition-selective pulses; (c) after the implementation of a Toffoli gate on the $|110\rangle$ state using pulses optimized by the genetic algorithm method.

For the Fredkin gate, the fidelity is > 0.9 for the area which falls under the data points $(0, \pm 7.8)$ and $(\pm 5.3, 0)$ which approximately forms an ellipse. The Toffoli gate has fidelity > 0.9 for the area inscribed by points $(-2.8, -13.4)$, $(5.5, 0)$, $(1.4, 12.2)$ and $(-5.5, 0)$. In general, all the gates optimized by the GA method are of high fidelity and are robust against both offset and pulse flip angle errors.

F. Comparison with previous experimental implementations

We compared the results of our optimization of the Fredkin and the Toffoli gates using GAs, with previous experimental NMR implementations that use transition-selective pulses [20, 21, 57]. The experimental NMR spectra of this comparison are shown in Figures 8-9 for a Fredkin gate and a Toffoli gate implemented on the $|110\rangle$ pseudopure state, respectively. All spectra were recorded after applying an IIX operation (*i.e.* a 90° pulse on the third qubit). Since the chemical shifts of the three fluorine qubits in our particular molecule cover a very large frequency bandwidth, we crafted special excitation Gaussian shaped transition selective pulses that are frequency modulated [58]. Using transition-selective pulses, the Fredkin gate was experimentally implemented with a fidelity of 0.72 and a pulse length of 242 ms. Using transition-selective pulses, the Toffoli gate was experimentally implemented with a fidelity of 0.76 and a pulse length of 168 ms. The fidelity of both the Fredkin and the Toffoli gates using the pulses crafted using the GA method was > 0.95 and the total pulse durations were substantially smaller, being 51 ms and 27 ms for the Fredkin and the Toffoli gates, respectively. Furthermore, as can be seen from the NMR spectra in Figures 8-9, the standard implementation of these three-qubit gates using transition-selective pulses leads to considerable errors due to decoherence during these long pulses as well as offset errors. The GA-optimized pulse sequences on the other hand, have a high fidelity and do not suffer from these errors.

IV. CONCLUSIONS

In summary, we have optimally designed and experimentally implemented the universal multi-qubit Toffoli and Fredkin gates on a three-qubit NMR quantum information processor. We used a global optimization method based on genetic algorithms to determine the optimal unitary transformations and generate the corresponding numerically optimized rf pulse profiles. We were able to find optimal constructions for these important three-qubit universal control gates, which are robust against pulse offset errors as well as errors that could arise due to decoherence. We were able to find gate decompositions which are based only on hard (short duration) rf pulses and delays, which take very short times to implement and are of high fidelity. Our gate decompositions are sufficiently general and can be used for other quantum computing hardwares as well. Although some of the optimization protocols took a long time to run, the obvious advantage is that once the optimal pulse sequence for a gate is found, it can be used later without any further optimization as long as one is working on the same quantum computer.

ACKNOWLEDGMENTS

All experiments were performed on Bruker Avance-III 600 MHz and 400 MHz FT-NMR spectrometers at the NMR Research Facility at IISER Mohali. K.D. acknowledges funding from DST India under Grant number EMR/2015/000556. A. acknowledges funding from DST India under Grant number EMR/2014/000297. H. S. acknowledges financial support from CSIR India. P. P. acknowledges funding from the Indian Academy of Sciences Bangalore India, under the Summer Research Fellowship Programme.

-
- [1] M. A. Nielsen and I. L. Chuang, *Quantum Computation and Quantum Information* (Cambridge University Press, Cambridge UK, 2000).
 - [2] A. Barenco, C. H. Bennett, R. Cleve, D. P. Divincenzo, N. Margolus, P. Shor, T. Sleator, J. A. Smolin, and H. Weinfurter, *Phys. Rev. A*, **52**, 3457 (1995).
 - [3] T. Sleator and H. Weinfurter, *Phys. Rev. Lett.*, **74**, 4087 (1995).
 - [4] M. Mottonen, J. J. Vartiainen, V. Bergholm, and M. M. Salomaa, *Phys. Rev. Lett.*, **93**, 130502 (2004).
 - [5] M. Mohammadi and M. Eshghi, *Quant. Inf. Process.*, **7**, 175 (2008).
 - [6] J. A. Smolin and D. P. DiVincenzo, *Phys. Rev. A*, **53**, 2855 (1996).
 - [7] H. Buhrman, R. Cleve, J. Watrous, and R. de Wolf, *Phys. Rev. Lett.*, **87**, 167902 (2001).
 - [8] H. F. Hofmann, *Phys. Rev. Lett.*, **109**, 020408 (2012).
 - [9] D. G. Cory, M. D. Price, W. Maas, E. Knill, R. Laflamme, W. H. Zurek, T. F. Havel, and S. S. Somaroo, *Phys. Rev. Lett.*, **81**, 2152 (1998).
 - [10] M. D. Reed, L. DiCarlo, S. E. Nigg, L. Sun, L. Frunzio, S. M. Girvin, and R. J. Schoelkopf, *Nature*, **482**, 382 (2012).
 - [11] G. J. Milburn, *Phys. Rev. Lett.*, **62**, 2124 (1989).
 - [12] J. Shamir, H. J. Caulfield, W. Micelli, and R. J. Seymour, *Appl. Opt.*, **25**, 1604 (1986).
 - [13] A. Peres, *Phys. Rev. A*, **32**, 3266 (1985).
 - [14] Y. Shi, *Quantum Inf. Comput.*, **3**, 84 (2003).
 - [15] H. F. Chau and F. Wilczek, *Phys. Rev. Lett.*, **75**, 748 (1995).
 - [16] V. V. Shende and I. L. Markov, *Quantum Inf. Comput.*, **9**, 461 (2009).
 - [17] S. S. Ivanov, P. A. Ivanov, and N. V. Vitanov, *Phys. Rev. A*, **91**, 032311 (2015).
 - [18] E. Zahedinejad, J. Ghosh, and B. C. Sanders, *Phys. Rev. Lett.*, **114**, 200502 (2015).
 - [19] E. Zahedinejad, J. Ghosh, and B. C. Sanders, *Phys. Rev. Appl.*, **6**, 054005 (2016).
 - [20] F. Xue, J.-F. Du, M.-J. Shi, X.-Y. Zhou, R.-D. Hand, and J.-H. Wu, *Chin. Phys. Lett.*, **19**, 1048 (2002).

- [21] J. Du, M. Shi, J. Wu, X. Zhou, and R. Han, *Phys. Rev. A*, **63**, 042302 (2001).
- [22] R. Das, T. Mahesh, and A. Kumar, *J. Magn. Reson.*, **159**, 46 (2002), ISSN 1090-7807.
- [23] J. Zhang, W. Liu, Z. Deng, Z. Lu, and G. L. Long, *J. Opt. B*, **7**, 22 (2005).
- [24] T. Monz, K. Kim, W. Hansel, M. Riebe, A. S. Villar, P. Schindler, M. Chwalla, M. Hennrich, and R. Blatt, *Phys. Rev. Lett.*, **102**, 040501 (2009).
- [25] V. M. Stojanovic, A. Fedorov, A. Wallraff, and C. Bruder, *Phys. Rev. B*, **85**, 054504 (2012).
- [26] A. Fedorov, L. Steffen, M. Baur, M. P. da Silva, and A. Wallraff, *Nature*, **481**, 170 (2012).
- [27] M.-F. Chen, Y.-F. Chen, and S.-S. Ma, *Quant. Inf. Process.*, **15**, 1469 (2016).
- [28] B. P. Lanyon, M. Barbieri, M. P. Almeida, T. Jennewein, T. C. Ralph, K. J. Resch, G. J. Pryde, J. L. O'Brien, A. Gilchrist, and A. G. White, *Nature Phys.*, **5**, 134 (2009).
- [29] M. Micuda, M. Sedlak, I. Straka, M. Mikova, M. Dusek, M. Jezek, and J. Fiurasek, *Phys. Rev. Lett.*, **111**, 160407 (2013).
- [30] M. Micuda, M. Mikova, I. Straka, M. Sedlak, M. Dusek, M. Jezek, and J. Fiurasek, *Phys. Rev. A*, **92**, 032312 (2015).
- [31] J. K. Moqadam, G. S. Welter, and P. A. A. Esquef, *Quant. Inf. Process.*, **15**, 4501 (2016).
- [32] M.-X. Luo, S.-Y. Ma, X.-B. Chen, and X. Wang, *Scientific Reports*, **5**, 16716 (2015).
- [33] T. Ono, R. Okamoto, M. Tanida, H. F. Hofmann, and S. Takeuchi, *Scientific Reports*, **7**, 45353 (2017).
- [34] E. Fortunato, M. Pravia, N. Boulant, G. Teklemariam, T. Havel, and D. Cory, *J. Chem. Phys.*, **116**, 7599 (2002).
- [35] Z. Tosner, T. Vosegaard, C. Kehlet, N. Khaneja, S. J. Glaser, and N. C. Nielsen, *J. Magn. Reson.*, **197**, 120 (2009).
- [36] T. Schulte-Herbruggen, R. Marx, A. Fahmy, L. Kauffman, S. Lomonaco, N. Khaneja, and S. J. Glaser, *Phil. T. Roy. Soc. A*, **370**, 4651 (2012).
- [37] R. L. Kosut, M. D. Grace, and C. Brif, *Phys. Rev. A*, **88**, 052326 (2013).
- [38] T.-M. Zhang, R.-B. Wu, F.-H. Zhang, T.-J. Tarn, and G.-L. Long, *IEEE Trans. Ctrl. Syst. Tech.*, **23**, 2018 (2015).
- [39] J. H. Holland, *Adaptation in Natural and Artificial Systems: An Introductory Analysis with Applications to Biology, Control, and Artificial Intelligence* (MIT Press, Boston USA, 1992).
- [40] S. Forrest, *Science*, **261**, 872 (1993).
- [41] R. Stadelhofer, W. Banzhaf, and D. Suter, *Art. Int. Engg. Des. Anal. Manufac.*, **22**, 285 (2008).
- [42] Y. Hardy and W.-H. Steeb, *Intl. J. Mod. Phys. C*, **21**, 1359 (2010).
- [43] J. Bang and S. Yoo, *J. Korean Phys. Soc.*, **65**, 2001 (2014).
- [44] J. C. Navarro-Munoz, H. C. Rosu, and R. Lopez-Sandoval, *Phys. Rev. A*, **74**, 052308 (2006).
- [45] G. Quiroz and D. A. Lidar, *Phys. Rev. A*, **88**, 052306 (2013).
- [46] V. S. Manu and A. Kumar, *Phys. Rev. A*, **86**, 022324 (2012).
- [47] V. S. Manu and A. Kumar, *Phys. Rev. A*, **89**, 052331 (2014).
- [48] A. M. Souza, G. A. Alvarez, and D. Suter, *Phys. Rev. Lett.*, **106**, 240501 (2011).
- [49] K. Jebari and M. Madiafi, *Int. J. Emerg. Sci.*, **3**, 333 (2013).
- [50] MATLAB, *Version 8.5.0 (R2015a)* (MathWorks Inc., Natick, Massachusetts, 2015).
- [51] D. G. Cory, M. D. Price, and T. F. Havel, *Physica D*, **120**, 82 (1998).
- [52] G. M. Leskowitz and L. J. Mueller, *Phys. Rev. A*, **69**, 052302 (2004).
- [53] H. Singh, Arvind, and K. Dorai, *Phys. Lett. A*, **380**, 3051 (2016), ISSN 0375-9601.
- [54] A. Uhlmann, *Rep. Math. Phys.*, **9**, 273 (1976).
- [55] R. Jozsa, *J. Mod. Optics*, **41**, 2315 (1994).
- [56] N. Linden, B. Herve, R. J. Carbajo, and R. Freeman, *Chem. Phys. Lett.*, **305**, 28 (1999).
- [57] S. Dogra, K. Dorai, and Arvind, *Phys. Rev. A*, **91**, 022312 (2015).
- [58] D. Das, S. Dogra, K. Dorai, and Arvind, *Phys. Rev. A*, **92**, 022307 (2015).